



# Posterior parietal cortex predicts upcoming movement in dynamic sensorimotor control

Yuhui Li<sup>a,1</sup> , Yong Wang<sup>a</sup>, and He Cui<sup>b,c,d,2</sup>

Edited by Ranulfo Romo, Universidad Nacional Autonoma de Mexico, Mexico City, D.F., Mexico; received October 21, 2021; accepted February 18, 2022

Interaction with a rapidly changing world relies on dynamically integrating sensory inflows and motor outflows. Numerous studies have shed light on sensorimotor transformations in the posterior parietal cortex (PPC), but most have emphasized reactive movements toward static targets, in which the relationship between the sensory cues and the motor goals is fixed, making it difficult to distinguish neural activity relating to the movement from that reflecting the stimulus. To resolve this, we recorded single-neuron activity from the PPC in monkeys performing a manual interception task in which the instantaneous stimulus location is decoupled from the impending movement direction by different target speeds. Intriguingly, the results suggest that the PPC explicitly conveys information concerned with the forthcoming movement, rather than the instantaneous stimuli, suggesting an intimate role in motor planning.

sensorimotor control | monkey | reaching | manual interception | single-unit activity

Although there is ample evidence that the posterior parietal cortex (PPC) plays a key role in linking sensation and action, its exact role in sensorimotor control has been long debated. An intense, persistent controversy is whether the PPC predominately integrates and converts sensory information into a map for elaborating appropriate movements (1) or plays a proactive role in motor preparation (2). Previous studies emphasized purely reactive movements toward static targets. In such a spatially fixed stimulus-response contingency, it is very difficult to disentangle neural activity predicting the resulting movement from that reflecting the stimuli. To reveal the exact role of the PPC in sensorimotor control requires more sophisticated behavioral paradigms in which motor parameters are not tightly linked to sensory cues.

In the present study, we have recorded single-neuron activity from the PPC in monkeys performing a flexible manual interception task (3). Here, we focus on two parietal areas segregated by the intraparietal sulcus: the inferior parietal area 7a and superior parietal area 5d. To intercept a moving target, a movement must be planned beforehand to compensate for neuromechanical/sensorimotor delays, requiring extrapolation of target motion and prediction about future limb states (4, 5). In this task, the outgoing motor commands for different target motion speeds are incongruent with the incoming sensory stimuli. Given this decoupling, the single-neuron tuning properties provided an opportunity to dissociate motor outflow from sensory inflow. Intriguingly, cells in area 7a exhibited invariant tuning to interceptive reaching directions but shifted tuning to instantaneous target location for different target motion speeds. However, such predictive coding seems not to be simple efference copy because it is relatively weaker in area 5d. In such a flexible stimulus-response contingency, area 7a explicitly conveys information regarding the impending movement, regardless of the current stimuli, suggesting that the PPC plays an intimate role in motor planning.

## Results

**Distinct Neuronal Representations in a Flexible Manual Interception Task.** The objective of this study is to separate the neuronal encoding of impending reach direction (or predicted target location at interception time) from the encoding of current target location. For this purpose, we trained two monkeys (C and G) to perform a flexible manual interception task (Fig. 1A). The task is characterized by the following: 1) no direct sensory cue is presented to instruct where and when the interception is to be made, yet the animals must make a prompt interception within 1,000 ms after the target's appearance; and 2) the target to be intercepted appears randomly, chosen from one of eight locations evenly spaced along a circular target moving path, and it moves at one of five angular velocities (two different speeds by two different directions, plus a static condition). Therefore, the animals must take both target speed and sensorimotor delays into account to intercept the target accurately. Accordingly, the neuronal encoding of

## Significance

Most studies in sensorimotor neurophysiology have utilized reactive movements to stationary goals pre-defined by sensory cues, but this approach is fundamentally incapable of determining whether the observed neural activity reflects current sensory stimuli or predicts future movements. In the present study, we recorded single-neuron activity from behaving monkeys engaged in a dynamic, flexible, stimulus-response contingency task that enabled us to distinguish activity co-varying with sensory inflow from that co-varying with motor outflow in the posterior parietal cortex.

Author affiliations: <sup>a</sup>Brain and Behavior Discovery Institute, Medical College of Georgia, Augusta University, Augusta, GA 30912; <sup>b</sup>Center for Excellence in Brain Science and Intelligent Technology, Institute of Neuroscience, Chinese Academy of Sciences, Shanghai 200031, China; <sup>c</sup>Shanghai Center for Brain and Brain-inspired Intelligence Technology, Shanghai 200031, China; and <sup>d</sup>University of Chinese Academy of Sciences, Beijing 100049, China

Author contributions: Y.L. and H.C. designed research; Y.L., Y.W., and H.C. performed research; Y.L. analyzed data; and Y.L. and H.C. wrote the paper.

The authors declare no competing interest.

This article is a PNAS Direct Submission.

Copyright © 2022 the Author(s). Published by PNAS. This article is distributed under [Creative Commons Attribution-NonCommercial-NoDerivatives License 4.0 \(CC BY-NC-ND\)](https://creativecommons.org/licenses/by-nc-nd/4.0/).

<sup>1</sup>Present address: Department of Biomedical Engineering, Duke University, Durham, NC 27708.

<sup>2</sup>To whom correspondence may be addressed. Email: cuihe@ion.ac.cn.

This article contains supporting information online at <http://www.pnas.org/lookup/suppl/doi:10.1073/pnas.2118903119/-DCSupplemental>.

Published March 21, 2022.

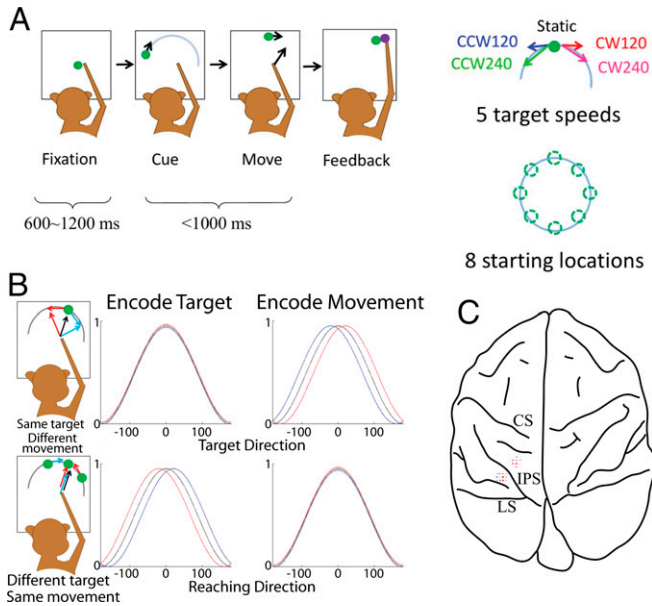


**Fig. 1.** Behavioral task (A), the theoretical prediction of two alternative neural encodings (B), and the in vivo recording sites (C). (A, Left) The flexible manual interception task. The light blue curve, which is not visible to the monkey, indicates the path of target motion. (Right) the 5 (motion speeds) by 8 (starting locations) design of the task. (B, Left) Under different target speed conditions, targets with the same instantaneous location (Upper left) triggered reaches in different directions, or reaches in the same direction are triggered by targets with different instantaneous locations (Bottom left); (Middle) the tuning curves and PDs when a neuron encodes instantaneous target location; (Right) when it encodes the movement goal. (Upper row) The tuning curves (and corresponding PDs) as a function of instantaneous target location; (Bottom row) those as a function of reaching direction. (C) A diagram showing the electrode penetration locations for in vivo recordings. The red dots and blue dots represent recording sites for monkey C and monkey G, respectively. The size of each dot represents recorded unit counts from that site. The anterior-medial cluster is recording sites for area 5d, and the posterior-lateral cluster is for area 7a. CS, central sulcus, IPS, intraparietal sulcus, LS, lateral sulcus.

predicted target location (thus, the interception direction) can be separated from the neuronal encoding of the current target location by comparing the variance of direction curves across different target speed conditions (Fig. 1B). If a neuron encodes the instantaneous location of the moving target, its activity should covary with target direction at reach onset, regardless of reaching direction. In such a case, the target-direction tuning curves should be invariant, whereas reaching-direction tuning curves should vary for reaches toward static, clockwise (CW), and counterclockwise (CCW) targets (Fig. 1B, Middle). On the other hand, a neuron that encodes the reach direction (predicted target location at interception) should be tuned to the actual reaching direction, regardless of current target location. Therefore, the neuron's target-direction tuning curves should shift for different target speed conditions, while its reaching-direction tuning curves should be invariant (Fig. 1B, Right).

**Examples of Typical Neurons.** We recorded single-unit activity from area 7a and area 5d in the PPC (Fig. 1C) while the animals were performing the interception task. We found that single-neuron activity in both brain regions was modulated by the behavioral task and varied across different task conditions, as exemplified in Fig. 2 by a typical area 7a neuron and a typical area 5d neuron. The firing rate of the area 7a neuron increased after the appearance of the target and peaked before onset of the interceptive reach (labeled as the black dots in raster plots in Fig. 2A). The firing rate gradually decreased after reach onset. The

firing rate was also modulated by target and/or reaching direction, which is obvious when comparing the firing rates in the static condition (the middle column in Fig. 2A).

To test whether the above neuron encoded the current target location or the reach direction, we replotted peri-stimulus time histograms (PSTHs) by grouping the trials either based on instantaneous target location at reach onset (Fig. 2C) or based on reaching direction (Fig. 2E). When trials are grouped by instantaneous target location, the firing rate profile to a particular instantaneous target location also depends on the target's speed (Fig. 2C). For example, while the instantaneous target was on the left side of the circle (the fifth row in Fig. 2C), the firing rate was higher when the target was moving CW than when the target was static or moving CCW. The opposite happened when the instantaneous stimulus was on the right side (first row). In contrast, the firing rate patterns were less variable across different target speed conditions when trials are grouped based on reaching direction (Fig. 2E).

The firing rate of the example area 5d neuron started to increase just before the onset of the reach movement and peaked during the movement (Fig. 2B, D, and F). Unlike the example area 7a neuron shown above, the area 5d neuron's tuning to instantaneous stimulus did not vary with target motion speed.

**Tuning Curve Fitting.** To quantify the variance in directional tunings across different target speed conditions for the above example neurons, we computed the firing rates at reach onset ( $\pm 50$  ms) and plotted them as a function of either the instantaneous target locations (scatter plots in upper row in Fig. 3A and B, for the area 7a and area 5d neurons, respectively) or the reaching directions (lower row) and then fitted the neural tunings with a circular version of a Gaussian function (the von Mises function; see *Materials and Methods*). The fitting process was applied to the data of each individual speed condition (colored lines in Fig. 3). From the Gaussian fitting results, we calculated the preferred direction (PD) as the angle at the peak of the fitting curve. If the neuronal tuning to a task/behavioral parameter is more independent of target speed, the PDs across different speed conditions should be less variable. The PDs of the target-direction tuning curves were separated as a function of target speed for the example area 7a neuron (top, Fig. 3A), while the PDs of the reaching-direction tuning curves were less variable (bottom, Fig. 3A). To illustrate the PD displacement as a function of target speed at the population level, we normalized the fitting curves of all neurons and centralized them by aligning their PDs in the static condition to zero degrees (see *Materials and Methods*), then averaged the normalized fitting curves under different target speeds. As shown in Fig. 3C, the population-averaged target-direction tuning curves and PDs of area 7a neurons were spread across different target speeds (upper left in Fig. 3C), while the reach-direction tuning curves and PDs were relatively similar (lower-left plot). This suggests that area 7a was better tuned to upcoming reaching direction than to instantaneous target location at the time of launching an interceptive reach.

To further characterize the dependency of target-/reach-directional tuning on target speeds for each neuron, we calculated variance of the PDs across different target speed conditions for reach-direction tuning ( $\text{VarPD}_{\text{reach}}$ ) as well as for target-direction tuning ( $\text{VarPD}_{\text{target}}$ ). Fig. 4 shows  $\text{VarPD}_{\text{target}}$  versus  $\text{VarPD}_{\text{reach}}$  for all recorded cells. In area 7a, the  $\text{VarPD}_{\text{reach}}$  was significantly smaller than the  $\text{VarPD}_{\text{target}}$  (Fig. 4A, Left;  $\text{VarPD}_{\text{target}} - \text{VarPD}_{\text{reach}}$ , mean  $\pm$  SD =  $0.07 \pm 0.13$ , Wilcoxon signed rank test,  $P < 10^{-6}$ ; also see Table 1).

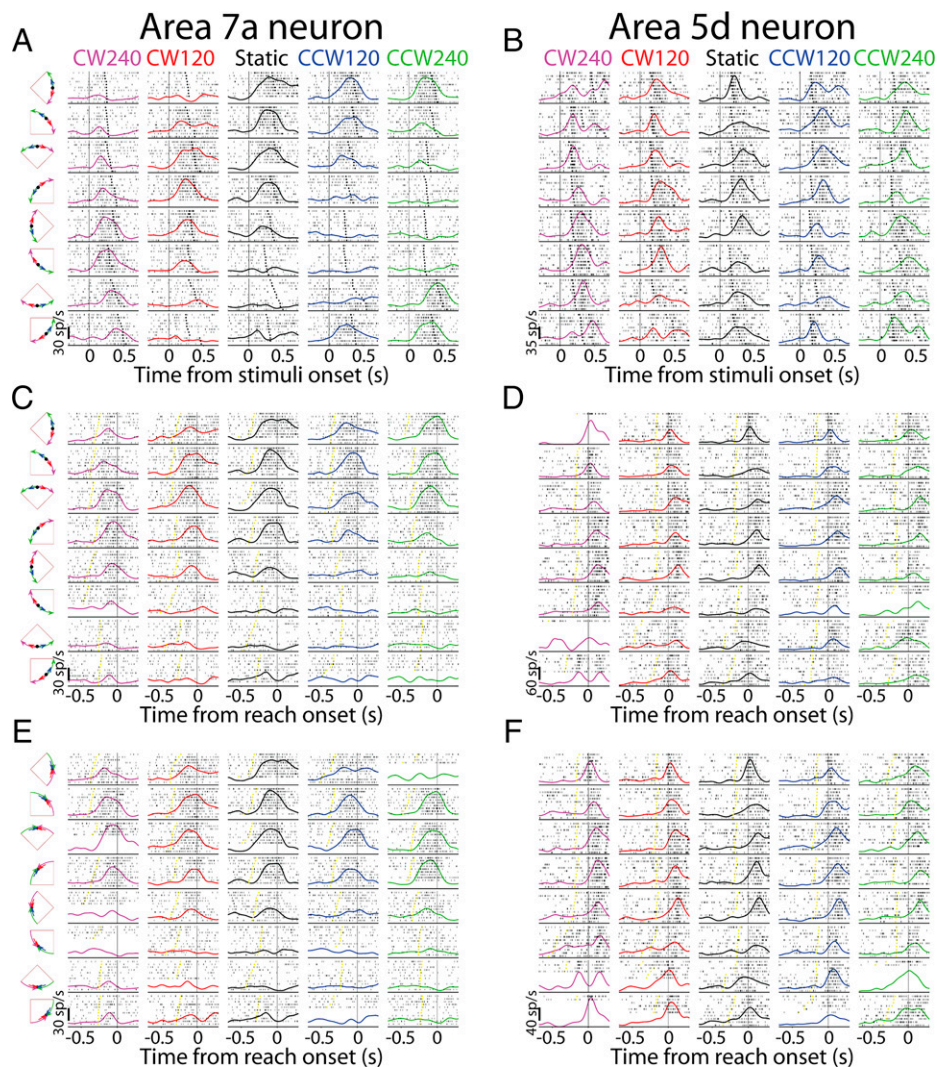


**Fig. 2.** The variance of the directional tuning by target moving speed in a typical area 7a neuron and a typical area 5d neuron. PSTHs of an area 7a neuron (*Left column*) and of an area 5d neuron (*Right column*). (A and B) Spike raster plots superimposed by PSTHs. The time is aligned to stimuli onset, and the reach onset times are indicated by black squares in the raster. The PSTHs were smoothed by a 50-ms Gaussian kernel. The trial conditions of stimulus starting locations (black dots) and moving speeds (colored arrows) are shown on the left. (C and D) Same data as shown in (A and B), but the PSTH and raster were recalculated by aligning time 0 to reach onset and by grouping the trials by the instantaneous target location at reach onset time into eight zones centered at 0°, 45°, 90°, 135°, 180°, 225°, 270°, and 315°. The target onset times are indicated by yellow squares in the raster. The trial conditions of instantaneous target locations (black dots) and moving speeds (colored arrows) are shown on the *Left*. (E and F) Same data of the neuron shown in (C and D), but the PSTHs and raster were recalculated by grouping the trials by reaching direction. The trial conditions of reaching directions (black dots) and target speeds (colored arrows) are shown on the *Left*.

To control for possible effects of eye movements on area 7a activity (6), we recorded 83 neurons from area 7a while the monkeys performed the flexible interception task with an eye-fixation requirement (eye-fixation condition, as compared to the above gaze-free condition). Consistent with the results in the gaze-free condition, in the eye-fixation condition, area 7a encoded reaching direction in a target speed-independent manner better than instantaneous target location, as reflected by the separation of target-direction tuning curves versus the overlapping of reach-direction tuning curves (left plots in Fig. 3D), as well as the smaller  $\text{VarPD}_{\text{reach}}$  compared to  $\text{VarPD}_{\text{target}}$  (Fig. 4B, *Left*;  $\text{VarPD}_{\text{target}} - \text{VarPD}_{\text{reach}} = 0.08 \pm 0.11$ ,  $P < 10^{-7}$ ).

The above results cannot be attributed to differences of the Gaussian fitting between target-direction tuning and reach-direction tuning because there was no significant difference between the two, either for goodness-of-fit (*SI Appendix*, Table 1) or for width of the fitting curve (*SI Appendix*, Table 2). These results are also robust with respect to the width of the time window chosen for calculating the firing rates at reach onset, as shown

by repeating the curve fitting with a wider window ( $\pm 100$  ms instead of  $\pm 50$  ms):  $\text{VarPD}_{\text{reach}}$  is smaller than  $\text{VarPD}_{\text{target}}$  in both the gaze-free ( $\text{VarPD}_{\text{target}} - \text{VarPD}_{\text{reach}} = 0.08 \pm 0.14$ ,  $P < 10^{-6}$ ) and the eye-fixation conditions ( $\text{VarPD}_{\text{target}} - \text{VarPD}_{\text{reach}} = 0.09 \pm 0.12$ ,  $P < 10^{-8}$ ). Furthermore, our results cannot be explained by area 7a encoding target location with a certain time lag due to sensory transmission delay. We tested the tuning on target location at 25 ms, 50 ms, 75 ms, 100 ms, and 150 ms before the reach onset and compared these to reach-direction tuning. We found that  $\text{VarPD}_{\text{reach}}$  was smaller than the  $\text{VarPD}_{\text{target}}$  for any time lag (gaze-free condition,  $\text{VarPD}_{\text{target}} - \text{VarPD}_{\text{reach}} = 0.09 \pm 0.15$ ,  $0.12 \pm 0.16$ ,  $0.15 \pm 0.17$ ,  $0.18 \pm 0.18$ ,  $0.24 \pm 0.20$  for 25 ms, 50 ms, 75 ms, 100 ms, and 150 ms, respectively;  $P < 10^{-7}$  for all cases. Eye-fixation condition,  $\text{VarPD}_{\text{target}} - \text{VarPD}_{\text{reach}} = 0.11 \pm 0.12$ ,  $0.14 \pm 0.14$ ,  $0.17 \pm 0.15$ ,  $0.21 \pm 0.17$ ,  $0.28 \pm 0.20$  for 25 ms, 50 ms, 75 ms, 100 ms, and 150 ms, respectively;  $P < 10^{-8}$  for all cases).

In area 5d, both the target-direction tuning curves and the reach-direction tuning curves were separated in the gaze-free

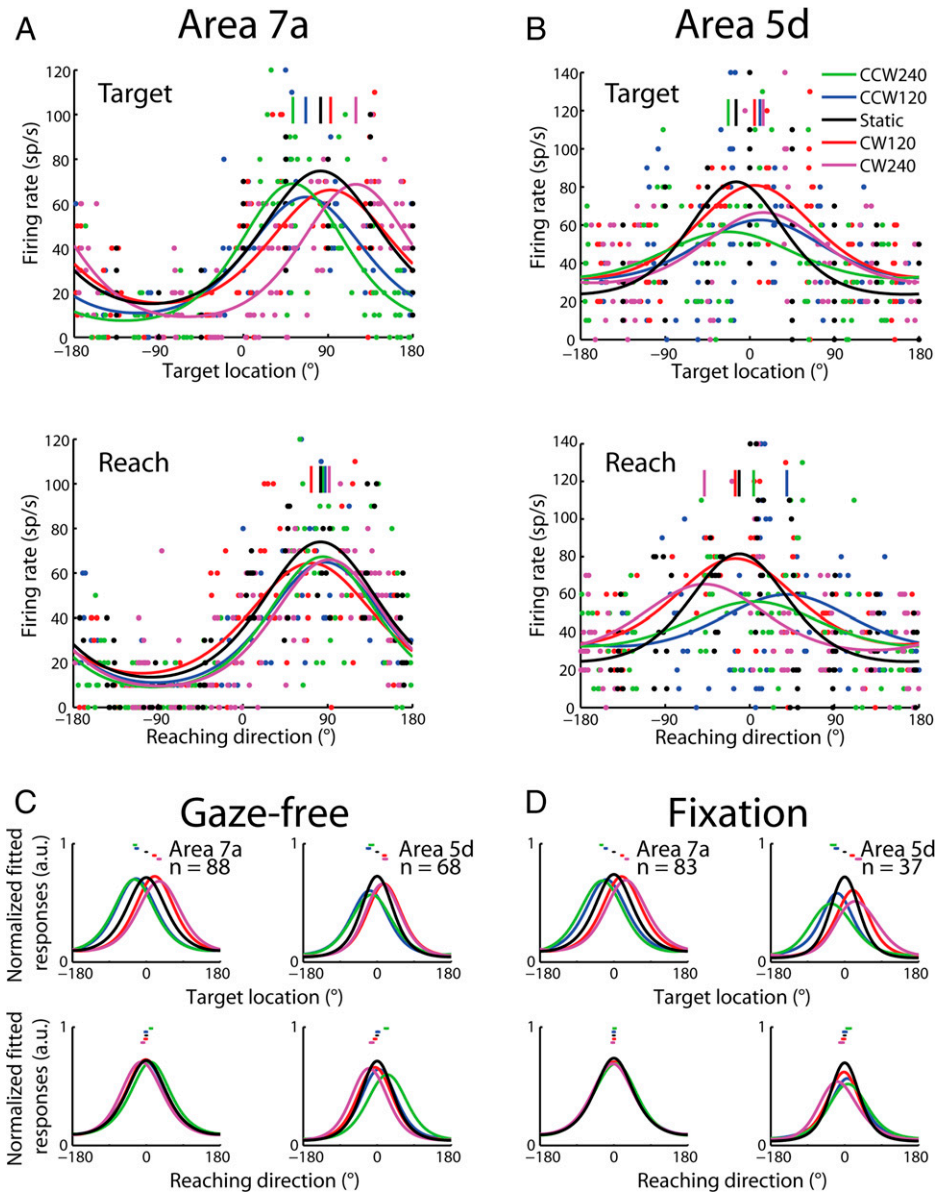


**Fig. 3.** Target versus movement tuning curves of example cells and the neuronal population. (A and B) The directional tuning data (scatters show the raw data points) and Gaussian fitting (solid lines) of the area 7a (A) and area 5d example cells (B) shown in Fig. 2. (Upper) Tuning as a function of instantaneous target location. (Bottom) Tuning as a function of reach direction. The colored lines show fitting curves for individual target speed conditions. The colored vertical lines on the top of individual fitting curves mark the PDs. (C and D) The population-averaged tuning curves in gaze-free (C) and eye-fixation conditions (D). The left (right) plots show results from area 7a (area 5d). The Upper (Bottom) row plots show target-direction (reach-direction) tuning curves. Each color in a plot corresponds to a target-speed condition. The colored bars above the curves indicate the mean  $\pm$  SEs of the PDs.

condition (Fig. 3C, Right). There was also no significant difference between  $\text{VarPD}_{\text{reach}}$  and  $\text{VarPD}_{\text{target}}$  (Fig. 4A, Right;  $\text{VarPD}_{\text{target}} - \text{VarPD}_{\text{reach}} = 0.04 \pm 0.15$ ,  $P = 0.12$ ). In the eye-fixation condition,  $\text{VarPD}_{\text{reach}}$  was significantly smaller than  $\text{VarPD}_{\text{target}}$  (Fig. 4B, Right), yet the difference was mainly contributed by one animal (see Table 1).

**Population Decoding.** To further compare stimulus versus movement information conveyed by area 7a and 5d at the population level, we trained a decoder, applying the method of support vector regression (7) to the firing rates and target locations in static (target speed = 0) and decoding target/movement directions in moving-target conditions (see Materials and Methods). The prediction errors were computed as the absolute angular difference between the predicted and actual reaching/target directions, as summarized in Fig. 5. Smaller error means better encoding. In both the gaze-free (A) and eye-fixation (B)

conditions, the results of population decoding showed that the decoder based on area 7a activity in the static trials predicted reaching direction much better than target location right before the interception of moving targets (Fig. 5 A and B, Left; prediction errors were significantly smaller for reach than for target, Wilcoxon rank sum test,  $P < 10^{-19}$  and  $P < 10^{-30}$  for gaze-free and eye-fixation conditions, respectively,  $n = 320, 10$  trials  $\times$  32 moving-target conditions), while such a trend was unclear for area 5d neurons (Fig. 6 A and B, Right; prediction errors were slightly smaller for reach than for target,  $P = 0.16$  and  $P = 0.02$  for gaze-free and eye-fixation condition, respectively). The difference in area 5d for the eye-fixation condition was mainly contributed by one monkey (see Table 2).

**Temporal Dynamics Analysis.** To further characterize evolution over time of the neuronal representation, we used a 100-ms sliding window with a 50-ms step to calculate the firing rates and

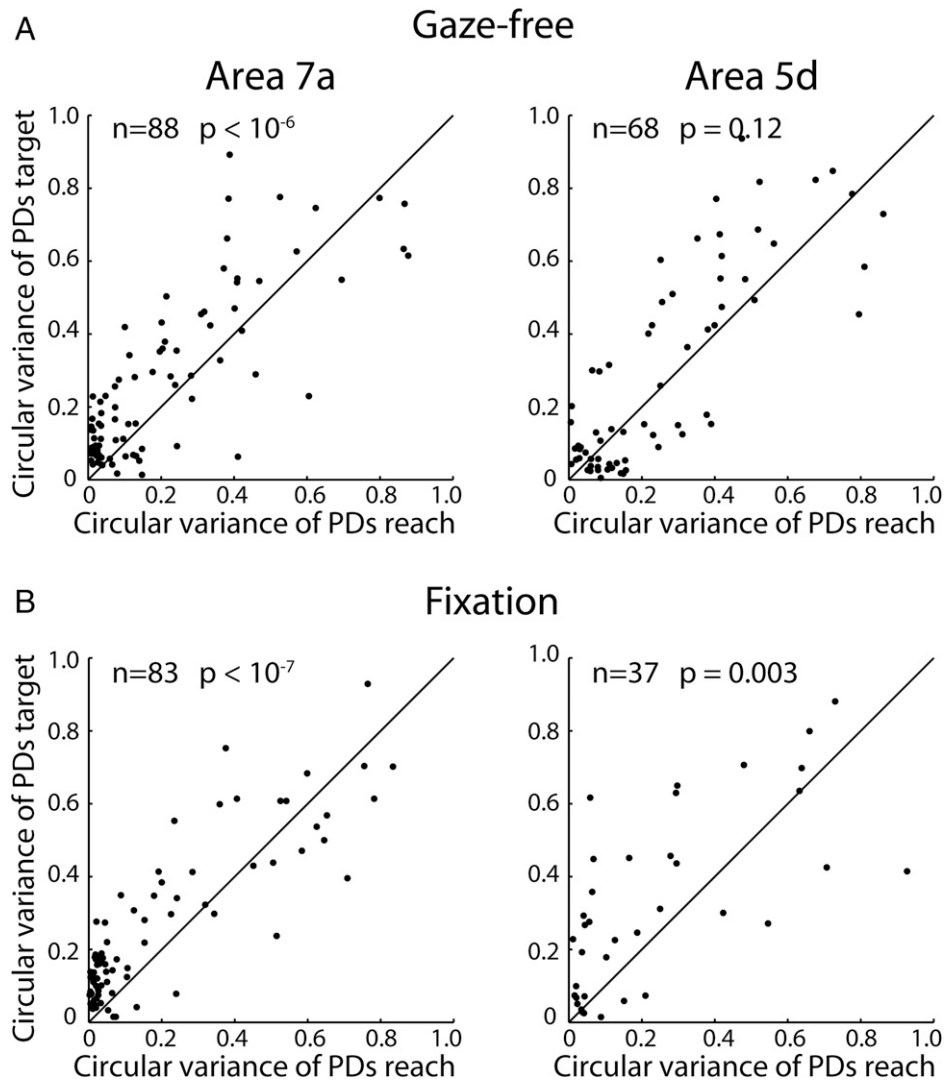


**Fig. 4.** Circular variance of the PDs of the Gaussian functions fitted to the turning curves of target location versus reach direction under different target speed conditions. (A) Scatterplots for PDs circular variance on target location turning versus reach direction turning in gaze-free condition. Each dot represents a cell. Area 7a results are shown on the *Left*, and area 5d results are shown on the *Right*. (B) Scatterplots for PDs circular variance on target-location turning versus reach-direction turning in the eye-fixation condition.

corresponding instantaneous target locations at different times from target or reach onset and performed the above PD variance analysis and population decoding. The results are shown in Fig. 6 (plot A–B for the PD variance and C–D for the population decoding result). In area 7a, the neural activity 100–150 ms after target onset represented instantaneous target location better than the future reaching direction, as reflected in both PD variance and population decoding (left plots in Fig. 6), even though at this time, the PD variance was relatively high, and the population decoding accuracy was relatively low. The area 7a activity represented future reaching direction better than instantaneous target location since ~50 ms prior to the reach onset. The activity in area 5d seemed to exhibit a tendency similar to that of area 7a, but the difference was less significant and less consistent across different task conditions and analysis methods.

## Discussion

Here, we recorded single-neuron activity from monkeys performing a flexible manual interception task that decoupled impending movement direction from current target location. Our purpose was to find out if the PPC best encodes instantaneous target

location or upcoming reach direction, by determining whether its neural activity modulation is invariant across different target speeds (Fig. 1B). Time-course analyses of spiking activity at both single-neuron (the tuning curves) and population (the population decoding) levels revealed that although the initial response in area 7a to target appearance seems sensory, its premovement activity represents the upcoming reaching direction better than the instantaneous target location. The results suggest that the PPC plays a proactive role in motor planning, rather than merely representing spatial target location.

While area 7a represents upcoming reach direction better than instantaneous target location, regardless of the eye-fixation requirement, such a preference was less clear in area 5d. These results are consistent with the previous finding that lesions in areas 7 and 5 impaired reaches in the light and dark, respectively (8). Area 7a is considered the top level of the dorsal visual hierarchy (9, 10). It is reciprocally connected with visual areas and other inputs from the prefrontal cortex, hippocampus, and cerebellum (9, 11), making it very likely to represent behaviorally relevant objects/locations in visual space. In contrast, area 5d receives a major cortical input from the primary somatosensory cortex (12, 13); is reciprocally connected with primary

**Table 1. Variance of PDs across different speed conditions**

	Circular variance					
	Area 7a					
	Gaze-free			Eye-fixation		
	Combined (n = 88)	Monkey C (n = 39)	Monkey G (n = 49)	Combined (n = 83)	Monkey C (n = 25)	Monkey G (n = 58)
Reach	0.17 ± 0.19	0.23 ± 0.22	0.12 ± 0.14	0.13 ± 0.18	0.09 ± 0.13	0.14 ± 0.19
Target	0.24 ± 0.21	0.31 ± 0.24	0.20 ± 0.17	0.21 ± 0.18	0.21 ± 0.19	0.21 ± 0.18
Target -Reach	0.07 ± 0.13	0.07 ± 0.17	0.07 ± 0.10	0.08 ± 0.11	0.12 ± 0.11	0.07 ± 0.10
P	< 10 <sup>-6</sup>	0.006	< 10 <sup>-4</sup>	< 10 <sup>-7</sup>	< 0.001	< 10 <sup>-5</sup>

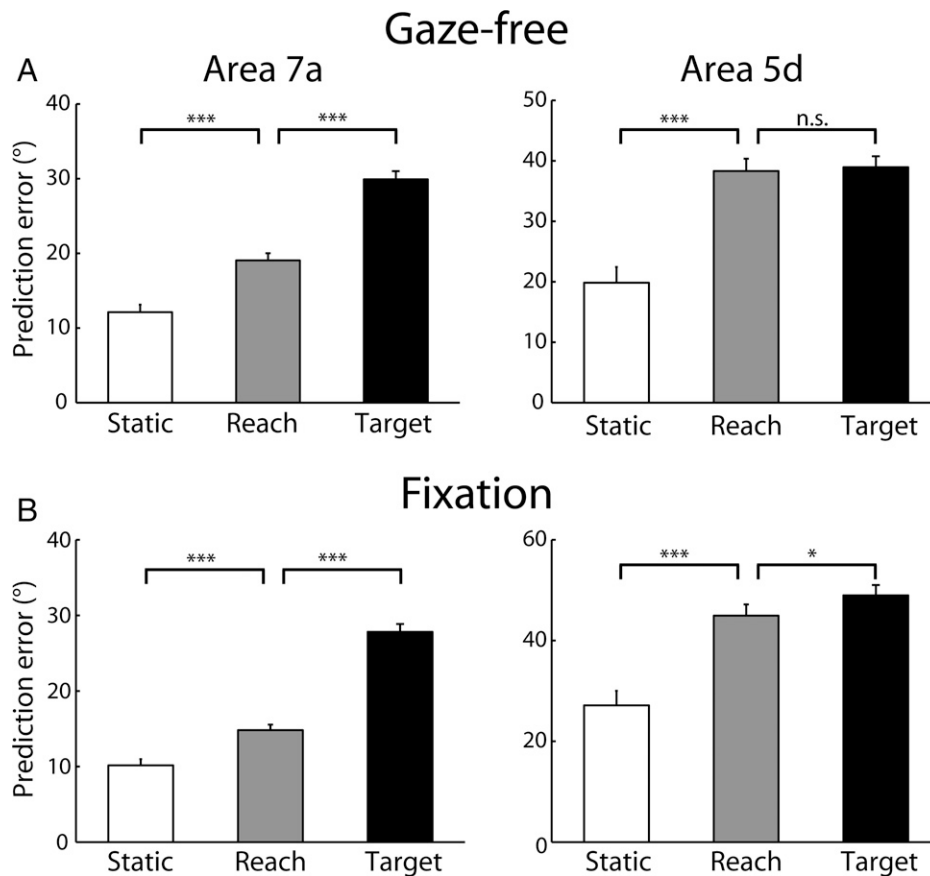
  

	Area 5d					
	Gaze-free			Eye-fixation		
	Combined (n = 68)	Monkey C (n = 43)	Monkey G (n = 25)	Combined (n = 37)	Monkey C (n = 23)	Monkey G (n = 14)
	Reach	0.21 ± 0.18	0.20 ± 0.15	0.21 ± 0.22	0.18 ± 0.20	0.20 ± 0.20
Target	0.25 ± 0.24	0.25 ± 0.24	0.24 ± 0.26	0.28 ± 0.22	0.35 ± 0.22	0.14 ± 0.13
Target -Reach	0.04 ± 0.15	0.05 ± 0.17	0.02 ± 0.13	0.10 ± 0.18	0.15 ± 0.18	-0.02 ± 0.13
P	0.12	0.18	0.41	0.003	0.002	1

The Wilcoxon signed rank test was used for statistical tests.

motor and premotor cortex (14); and is sensitive to the kinematic (15), but not the dynamic, characteristics of active arm movements (16). Therefore, in our task, more information

regarding upcoming movements was encoded in area 7a, probably because the task was, essentially, a visually guided manual interception (17). In contrast, area 5d is more involved in the



**Fig. 5.** Prediction errors of impending reach direction or instantaneous target location by support vector regression. (A) Prediction errors in static trials (white bars, in static target trials), reach direction in nonstatic target trials (gray bars), and instantaneous target location in nonstatic target trials in gaze-free condition. Area 7a results are shown on the *Left*, and area 5d results are shown on the *Right*. (B) Prediction errors in eye-fixation condition. Error bars represent SEs. \*\*\*:  $P < 0.001$ ; \*:  $P < 0.05$ ; n.s.: non significant.

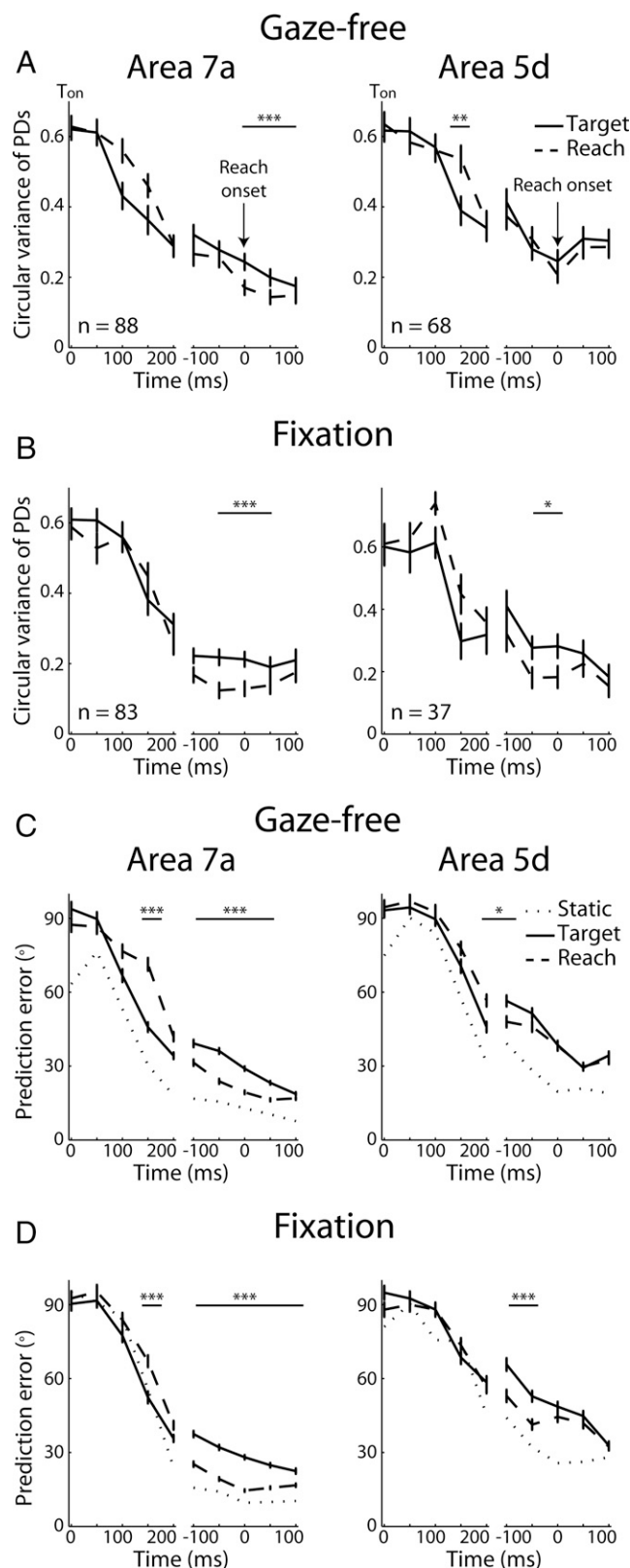


**Fig. 6.** Temporal dynamics of the circular variance of the PDs and prediction errors of population decoding. (A and B) Population-averaged circular variance of PDs over time in the gaze-free task (A) and the eye fixation task (B). The *Left* (*Right*) plots show results from area 7a (area 5d). The solid and dashed lines show results from fitting the target-location and reach-direction tuning curves, respectively. The vertical lines in the plots show mean  $\pm$  SEs. (C and D) Prediction errors of population decoding over time in gaze-free (C) and eye-fixation (D) conditions. The *Left* (*Right*) plots show results from area 7a (area 5d). The dotted lines, solid lines, and dashed lines show the prediction errors of decoding the target location in the static condition, the instantaneous target location in the non-static condition, and

motor execution (18, 19). One possibility is that activity in area 5d is modulated by details of the configuration of the movement (20, 21), so the activity was also modulated by factors such as movement velocity, which was affected by target speed.

Flexible manual interception, which requires that the hand is displaced to the right location at the right time, relies on the prediction of future target location at movement offset, based on the extrapolation of target motion (22, 23) in accordance with movement duration. Converging evidence supports the idea that area 7a encodes attended location due to top-down mechanisms (24, 25). Activity in area 7a that covaries with impending interceptive reach might also incorporate inputs from frontal motor cortex and underlie attention directed at the reaching goal, as predicted by the theory of premotor attention (26). Merchant and colleagues (27, 28) found that when monkeys watched a target moving rapidly along a circular path, or intercepted it at a predefined location (six o'clock), a large population of area 7a neurons exhibited angular tuning incongruent with their static response fields. From our point of view, such shifted angular tuning might reflect predictive encoding made continually available for upcoming action, even in the absence of actual motor responses.

Any explanation that accounts for the behavioral fact that animals routinely intercept moving targets must incorporate a forward model to compensate for inherent sensorimotor delays in motor control (29–32). For flexible manual interception, if the monkey is well trained, the desired reach endpoint, presumably, is the predicted location of the moving target at reach offset. As a crucial node incorporating visual, proprioceptive, and efference copy information in a sensorimotor network (33), the PPC is a plausible candidate for mediating the fundamental relationship between sensory prediction and motor control. Although our results suggested that PPC activity predicts future arm/hand position rather than reflecting the concurrent sensory stimulus, it is difficult to claim that this activity is the neural correlate of the forward model because the internal prediction of a future event is difficult to measure behaviorally. Recent evidence (34) has suggested that areas 5 and 7 provide signals to compensate for motor and target errors, respectively, raising the possibility that PPC activity might encode prediction error in addition to target location. However, because our monkeys were well trained to perform their task ( $\sim 90\%$  correct), leading to small errors (monkey C: mean  $\pm$  SD =  $0.8^\circ \pm 7.9^\circ$ ; monkey G:  $-0.1^\circ \pm 10.3^\circ$ ) compared to neuronal tuning (tuning width =  $130\sim 140^\circ$ ), it is hard to determine whether the PPC also carries error information in the present study. Therefore, pinpointing the neural substrate of the forward model demands more sophisticated behavioral paradigms and experimental interventions than have been thus far implemented.

## Materials and Methods

**Animals.** Two adult male rhesus monkeys (monkey C and monkey G, *Macaca mulatta*, 7–10 kg) were used in the study. All animal maintenance and procedures were in accordance with NIH guidelines and were approved by the Institutional Animal Care and Use Committee (IACUC) of Augusta University.

**Behavioral Task.** The monkeys were trained to perform a visual-guided reaching interception task, as described in a previous study (3). Specifically, a trial was

the reaching direction in the non-static condition, respectively. The vertical lines in the plots show mean  $\pm$  SEs. For all plots in C and D,  $n = 320$  (32 task conditions by 10 trials). \*\*\*:  $P < 0.001$ ; \*\*:  $P < 0.01$ ; \*:  $P < 0.05$  after Bonferroni correction to adjust for multiple comparisons.

**Table 2. Prediction errors by decoders trained by support vector regression**

	Prediction errors (°)					
	Area 7a					
	Gaze-free			Eye-fixation		
	Combined	Monkey C	Monkey G	Combined	Monkey C	Monkey G
Static	12.1 ± 9.1	22.3 ± 16.9	15.3 ± 11.3	10.2 ± 7.4	27.9 ± 23.4	11.8 ± 9.1
Reach	19.1 ± 17.1	31.4 ± 30.1	20.1 ± 18.2	14.8 ± 13.1	31.1 ± 30.3	14.6 ± 13.0
Target	29.9 ± 19.7	35.9 ± 30.0	31.8 ± 25.6	27.8 ± 18.6	41.3 ± 33.0	26.4 ± 17.6
<i>P</i>	< 10 <sup>-19</sup>	0.01	< 10 <sup>-11</sup>	< 10 <sup>-30</sup>	< 10 <sup>-6</sup>	< 10 <sup>-24</sup>
	Area 5d					
	Gaze-free			Eye-fixation		
	Combined	Monkey C	Monkey G	Combined	Monkey C	Monkey G
	Static	19.8 ± 23.4	25.6 ± 34.8	32.4 ± 30.3	27.1 ± 25.7	30.9 ± 31.4
Reach	38.3 ± 36.1	42.6 ± 40.3	46.3 ± 42.2	44.9 ± 40.1	48.4 ± 42.6	59.8 ± 45.6
Target	38.9 ± 32.3	44.5 ± 37.5	46.1 ± 40.2	49.0 ± 36.9	55.2 ± 43.6	59.6 ± 46.2
<i>P</i>	0.16	0.18	0.86	0.02	0.02	0.91

The Wilcoxon rank sum test was used for statistical tests.

initiated when the monkey touched a dot on the center of a touch screen for 600–1200 ms (Fig. 1A). Then, a green target circle appeared and moved along the circle (the moving path was invisible to the monkey) for 1,000 ms. The monkey could intercept the target at any moment within 150–950 ms after target appearance. Once any peripheral location was touched, the target stopped. If the angle between the target and the hand endpoint was less than 15°, the interception was considered successful, and the monkey was rewarded. The interception target initially appeared at one of eight peripheral locations distributed evenly along the circular path and moved in one of five angular velocities: 0 (static), 120°/s or 240°/s CW, or 120°/s or 240°/s CCW. The 40 trial types (8 target starting positions × 5 target angular velocities) were pseudorandomly interleaved. Unsuccessful trials were pseudorandomly repeated until success was achieved. Two different conditions of the task were used. In the gaze-free condition, the monkeys could freely direct their gaze. After all neuronal recording sessions in the gaze-free condition were completed, the monkeys were trained to maintain their gaze on a red circle in the center of the touch screen throughout the trial (eye-fixation condition), and data were then collected for this condition. Visual stimuli were generated by VisionEgg (35). LabView (National Instrument) was used to monitor/control the monkeys' behavioral performance. Parts of the behavioral results have been previously published (3).

**Surgery.** After the monkeys were adequately trained on the interception task (accurate rate > 90% in the gaze-free condition), a headpost and a recording chamber (inner diameter = 19 mm) were implanted stereotaxically under anesthesia (introduced by 10 mg/kg ketamine, then sustained by 2% isoflurane). The center of the recording chamber was posterior 6.0 mm and lateral 11.0 mm in stereotaxic coordinates in order to cover the intraparietal sulcus (IPS) in the left hemisphere.

**Data Collection.** A magnetic sensor (Polhemus, sampling rate 120 Hz) was attached on the right arm near the wrist to track the hand trajectory. Eye movements were monitored by an infrared eye-tracker (ISCAN, 120 Hz). For electrophysiological recording, we lowered glass-coated tungsten electrodes (Alpha-Omega, ~1 MΩ impedance at 1 kHz) through a grid matrix in the recording chamber into the gyral surface of the superior parietal lobule (area 5d) and inferior parietal lobule (area 7a). The recording sites of area 5d were located between 0 and 3 mm anterior-medial to the IPS and between 7 and 11 mm from the midline. The recording sites for area 7a were located between 0 and 3 mm posterior-lateral to the IPS and between 11 and 15 mm from the midline (see Fig. 1C for a mapping of the coordinates all the recording sites on an illustration of the monkey brain). Due to the placement of the recording chamber and the electrode manipulators, some cells may be sampled from area 7b close

to the border with area 7a. The recording depths for both brain regions were limited to within 2 mm from the first encounter of neuronal activity. The area 5d units were confirmed by strong responses to passive somatic stimulation of the upper limbs. The area 7a units were confirmed by visual stimulation. Extracellular activity was recorded with the AlphaMap system (Alpha-Omega, sampling rate 50 kHz, filtered at 300–10 kHz).

**Data Analysis.** Spikes were extracted and sorted off-line using open-source software (36). For the purpose of the current study, we define a neuron to be task related if its responses are significantly different in conditions when static targets initially appeared at eight different locations (ANOVA, *P* < 0.05) either 50~250 ms after target appearance or -100~100 ms relative to reach onset (the directional tuning to static targets is tested for significance by calculating the *r* value and comparing the distribution of *r* values with a boot-strap resampling process: >95% of the distribution indicates significance). Consequentially, 171 area 7a neurons (monkey C: 64 from 89 recorded neurons, 71.9%; monkey G: 107 from 167 recorded neurons, 64.1%) and 105 area 5d neurons (monkey C: 66/87, 75.9%; monkey G: 39/71, 54.9%) were deemed to be task related. Of these, 88 area 7a cells (monkey C: 39, monkey G: 49) and 68 area 5d cells (monkey C: 43, monkey G: 25) were recorded in the gaze-free condition, and 83 area 7a cells (monkey C: 25, monkey G: 58) and 37 area 5d cells (monkey C: 23, monkey G: 14) were recorded in the eye-fixation condition. The data from the gaze-free condition and that from the eye-fixation conditions were from two nonoverlapping groups of neurons.

The firing rates of each cell at reach onset (±50 ms) were plotted as a function of either the instantaneous target location or the reaching direction. Then, they were fitted by a circular version of a Gaussian function:  $R = A + B \cdot \exp(C \cdot \cos(\theta - \theta_0))$ , where *R* is the firing rate in the time window of interest in a trial; *A* is the baseline; *B* determines the directional tuning depth; *C* determines the tuning width;  $\theta$  is the direction (target or movement) in that trial; and  $\theta_0$  is the direction corresponding to the peak of the curve, which is also the PD. The MatLab function "nlinfit" was used for fitting. Because the distributions of the firing rate data were identical for the reach-direction curve and for the target location for each cell, the baseline firing rates should be the same, so after initial fittings for both curves, we compared the resulting parameter *A*, then averaged *A* and fixed it, and did the fitting again to get the result. After the fitting, the tuning width is characterized by the full width at half maximal (FWHM), which was calculated from the fitting resultant parameter *C*:  $FWHM = 2 \cdot \cos(\ln(\cosh(C))/C)$ . The circular variance of PDs was calculated by the function "circ\_var" from the MatLab "CircStat" toolbox. To calculate the population-averaged tuning curves shown in Fig. 3 C and D, the Gaussian fitting curves of individual neurons were normalized to have unity area under the tuning curve and centralized to locate

the PD of the fitting curve of the static condition at zero degrees. Then, these standardized curves were averaged across the neuronal population. The mean and SEs of the PD of the standardized curves were also computed.

Population decoding was done by using the method of support vector regression (7). The decoder was first trained by the firing rates and the target locations in static (target speed = 0) trials using the MatLab function "fitsvm." Then, the firing rates from moving-target trials were applied to the trained decoders to predict target/movement directions (using the MatLab function "predict"). The prediction errors were computed as the absolute angular difference between the predicted and the actual reaching or the instantaneous target directions. To make the support vector regression applicable to the angular variable of reach direction (or target location), we converted the angular variable to two linear variables,  $x = \cos(\theta)$  and  $y = \sin(\theta)$ , and trained two independent decoders for  $x$  and  $y$ , respectively. Subsequently, the decoders predicted  $x'$  and  $y'$ , and the predicted directions were computed as  $\theta' = \text{angle}(x' + y' * i)$ , where  $i$  is the imaginary unit. Both the training and the predicting processes were based on the "population" firing rates of all recorded neurons from area 7a or 5d. Because the firing rates of different cells were usually recorded from different sessions, in order to train decoders robustly representing the relation between task variables and the corresponding population firing rate patterns, we first sorted firing rates of all cells from all trials from the same behavioral condition (target location in static conditions) so that the firing rates of each cell in each trial were combined with the firing rates of a trial of all other cells to form one population firing rate pattern of that behavioral condition. Then, we randomly shuffled the grouping among trials of all cells to augment the size of the dataset to 100 times of the original dataset and used the whole dataset to train the decoder. In the decoding, we derived the population firing rate patterns by sorting firing rates of different cells in trials with the same behavioral condition (target starting location). However, here, no data augment was used. We confirmed that the variance of the task variables (reach direction or instantaneous target location) in trials where the firing rates of different cells were aligned into individual population firing rate patterns was small. The above variance was also comparable between the

two task variables (small and no significant difference). Statistics of the prediction errors were performed by pooling all trials from the non-static conditions (4 target motion speeds by 8 starting locations). To estimate the decoder's baseline performance for static condition data, the training data were divided into 10 sets for the leave-one-out strategy. Each time, 9 sets of the data were used to train the decoder, and the remaining set was used to compute the prediction errors. The procedure was repeated 10 times, so each set of the data was used as the testing data once. The average of the 10 sets of prediction errors was used as a reference for the decoder's baseline performance.

To reveal the temporal dynamics of the neural representation, a 100-ms sliding window with a 50-ms step was used to compute the firing rates within different time intervals relative to target or reach onset (Fig. 6). The corresponding instantaneous target location was also calculated. Then, the curve-fitting and population-decoding analyses described above were repeated, based on the instantaneous firing rates, instantaneous target location, and final reaching direction. For the statistics in Fig. 6, the Bonferroni correction was used to adjust for multiple comparisons.

**Data Availability.** Anonymized data [electroneurophysiological data] have been deposited on Mendeley, <https://data.mendeley.com/datasets/j73ssvsnxy/1>.

**ACKNOWLEDGMENTS.** We thank E. Tsien for assistance during animal training; D. Blake, Y. Chen, J. Malpeli, A. Saul, T. Wang, Y. Zhang, C. Zheng, and R. Zheng for helpful comments and discussions; N. Rodriguez, M. Williams-Fritze, S. Cozzi, and P. Charlton for veterinary assistance; and P. Ding, A. Gambill, T. Goodly, and L. Jarrett for administrative support. This work was supported by National Key R&D Program (Grant 2017YFA0701102), National Science Foundation of China (Grants 31871047 and 31671075), Shanghai Municipal Science and Technology Major Project (Grant 2021SHZDZX), CAS Strategic Priority Research Program (Grant XDB32040103), Lingang Lab (Grant LG202105-01-02), the Whitehall Foundation award, and Alfred P. Sloan Research Fellowship to H.C.

1. J. W. Bisley, M. E. Goldberg, Attention, intention, and priority in the parietal lobe. *Annu. Rev. Neurosci.* **33**, 1–21 (2010).
2. R. A. Andersen, H. Cui, Intention, action planning, and decision making in parietal-frontal circuits. *Neuron* **63**, 568–583 (2009).
3. Y. Li, Y. Wang, H. Cui, Eye-hand coordination during flexible manual interception of an abruptly appearing, moving target. *J. Neurophysiol.* **119**, 221–234 (2018).
4. J. F. Soechting, M. Flanders, Extrapolation of visual motion for manual interception. *J. Neurophysiol.* **99**, 2956–2967 (2008).
5. M. Zago, J. McIntyre, P. Senot, F. Lacquaniti, Visuo-motor coordination and internal models for object interception. *Exp. Brain Res.* **192**, 571–604 (2009).
6. R. A. Andersen, G. K. Essick, R. M. Siegel, Encoding of spatial location by posterior parietal neurons. *Science* **230**, 456–458 (1985).
7. V. Vapnik, *The Nature of Statistical Learning Theory* (Springer Science & Business Media, 2013).
8. M. F. Rushworth, P. D. Nixon, R. E. Passingham, Parietal cortex and movement. II. Spatial representation. *Exp. Brain Res.* **117**, 311–323 (1997).
9. R. A. Andersen, C. Asanuma, G. Essick, R. M. Siegel, Corticocortical connections of anatomically and physiologically defined subdivisions within the inferior parietal lobule. *J. Comp. Neurol.* **296**, 65–113 (1990).
10. D. J. Felleman, D. C. Van Essen, Distributed hierarchical processing in the primate cerebral cortex. *Cereb. Cortex* **1**, 1–47 (1991).
11. D. A. Crowe *et al.*, Prefrontal neurons transmit signals to parietal neurons that reflect executive control of cognition. *Nat. Neurosci.* **16**, 1484–1491 (2013).
12. E. G. Jones, J. D. Coulter, S. H. Hendry, Intracortical connectivity of architectonic fields in the somatic sensory, motor and parietal cortex of monkeys. *J. Comp. Neurol.* **181**, 291–347 (1978).
13. R. C. Pearson, T. P. Powell, The projection of the primary somatic sensory cortex upon area 5 in the monkey. *Brain Res.* **356**, 89–107 (1985).
14. P. L. Strick, C. C. Kim, Input to primate motor cortex from posterior parietal cortex (area 5). I. Demonstration by retrograde transport. *Brain Res.* **157**, 325–330 (1978).
15. J. Ashe, A. P. Georgopoulos, Movement parameters and neural activity in motor cortex and area 5. *Cereb. Cortex* **4**, 590–600 (1994).
16. J. F. Kalaska, D. A. Cohen, M. Prud'homme, M. L. Hyde, Parietal area 5 neuronal activity encodes movement kinematics, not movement dynamics. *Exp. Brain Res.* **80**, 351–364 (1990).
17. W. A. MacKay, Properties of reach-related neuronal activity in cortical area 7A. *J. Neurophysiol.* **67**, 1335–1345 (1992).
18. H. Cui, R. A. Andersen, Different representations of potential and selected motor plans by distinct parietal areas. *J. Neurosci.* **31**, 18130–18136 (2011).
19. Y. Li, H. Cui, Dorsal parietal area 5 encodes immediate reach in sequential arm movements. *J. Neurosci.* **33**, 14455–14465 (2013).
20. C. A. Buneo, M. R. Jarvis, A. P. Batista, R. A. Andersen, Direct visuomotor transformations for reaching. *Nature* **416**, 632–636 (2002).
21. S. H. Scott, L. E. Sergio, J. F. Kalaska, Reaching movements with similar hand paths but different arm orientations. II. Activity of individual cells in dorsal premotor cortex and parietal area 5. *J. Neurophysiol.* **78**, 2413–2426 (1997).
22. C. Bourrelly, J. Quinet, L. Goffart, The caudal fastigial nucleus and the steering of saccades toward a moving visual target. *J. Neurophysiol.* **120**, 421–438 (2018).
23. V. P. Ferrera, A. Barborica, Internally generated error signals in monkey frontal eye field during an inferred motion task. *J. Neurosci.* **30**, 11612–11623 (2010).
24. M. V. Chafee, B. B. Averbeck, D. A. Crowe, Representing spatial relationships in posterior parietal cortex: Single neurons code object-referenced position. *Cereb. Cortex* **17**, 2914–2932 (2007).
25. D. A. Crowe, M. V. Chafee, B. B. Averbeck, A. P. Georgopoulos, Neural activity in primate parietal area 7a related to spatial analysis of visual mazes. *Cereb. Cortex* **14**, 23–34 (2004).
26. G. Rizzolatti, L. Riggio, I. Dascola, C. Umiltà, Reorienting attention across the horizontal and vertical meridians: Evidence in favor of a premotor theory of attention. *Neuropsychologia* **25** (1A), 31–40 (1987).
27. H. Merchant, A. Battaglia-Mayer, A. P. Georgopoulos, Neural responses during interception of real and apparent circularly moving stimuli in motor cortex and area 7a. *Cereb. Cortex* **14**, 314–331 (2004).
28. H. Merchant, A. Battaglia-Mayer, A. P. Georgopoulos, Neural responses in motor cortex and area 7a to real and apparent motion. *Exp. Brain Res.* **154**, 291–307 (2004).
29. K. P. Körding, D. M. Wolpert, Bayesian integration in sensorimotor learning. *Nature* **427**, 244–247 (2004).
30. R. Nijhawan, Motion extrapolation in catching. *Nature* **370**, 256–257 (1994).
31. P. N. Sabes, The planning and control of reaching movements. *Curr. Opin. Neurobiol.* **10**, 740–746 (2000).
32. E. Todorov, Optimality principles in sensorimotor control. *Nat. Neurosci.* **7**, 907–915 (2004).
33. C. A. Buneo, R. A. Andersen, The posterior parietal cortex: Sensorimotor interface for the planning and online control of visually guided movements. *Neuropsychologia* **44**, 2594–2606 (2006).
34. M. Inoue, S. Kitazawa, Motor error in parietal area 5 and target error in area 7 drive distinctive adaptation in reaching. *Curr. Biol.* **28**, 2250–2262.e3 (2018).
35. A. D. Straw, Vision egg: An open-source library for realtime visual stimulus generation. *Front. Neuroinform.* **2**, 4 (2008).
36. R. Q. Quiroga, Z. Nadasdy, Y. Ben-Shaul, Unsupervised spike detection and sorting with wavelets and superparamagnetic clustering. *Neural Comput.* **16**, 1661–1687 (2004).